

Effects of Inclination on Measuring Velocity Dispersion and Implications for Black Holes

Jillian M. Bellovary^{1,2*}, Kelly Holley-Bockelmann^{1,2}, Kayhan Gültekin³, Charlotte R. Christensen⁴, Fabio Governato⁵, Alyson M. Brooks⁶, Sarah Loebman³, Ferah Munshi⁷

¹*Department of Physics and Astronomy, Vanderbilt University, PMB 401807, Nashville, TN, 37206, USA*

²*Department of Natural Sciences and Mathematics, Fisk University, 1000 17th Avenue N., Nashville, TN 37208, USA*

³*Department of Astronomy, University of Michigan, 830 Dennison, 500 Church St., Ann Arbor, MI, 48109, USA*

⁴*Department of Astronomy, University of Arizona, 933 North Cherry Avenue, Rm. N204, Tucson, AZ, 85721, USA*

⁵*Department of Astronomy, University of Washington, Box 351580, Seattle, WA, 98195, USA*

⁶*Department of Physics and Astronomy, Rutgers University, 136 Frelinghuysen Rd, Piscataway, NJ, 08854, USA*

⁷*Department of Physics and Astronomy, University of Oklahoma, 440 W. Brooks St., Norman, OK, 73019, USA*

6 December 2024

ABSTRACT

The relation of central black hole mass and stellar spheroid velocity dispersion (the $M - \sigma$ relation) is one of the best-known and tightest correlations linking black holes and their host galaxies. There has been much scrutiny concerning the difficulty of obtaining accurate black hole measurements, and rightly so; however, it has been taken for granted that measurements of velocity dispersion are essentially straightforward. We examine five disk galaxies from cosmological SPH simulations and find that line-of-sight effects due to galaxy orientation can affect the measured σ_{los} by 30%, and consequently black hole mass predictions by up to 1.0 dex. Face-on orientations correspond to systematically lower velocity dispersion measurements, while more edge-on orientations give higher velocity dispersions, due to contamination by disk stars when measuring line of sight quantities. We caution observers that the uncertainty of velocity dispersion measurements is at least 20 km s^{−1}, and can be much larger for moderate inclinations. This effect may account for some of the scatter in the locally measured $M - \sigma$ relation, particularly at the low-mass end.

Key words: galaxies: bulges, galaxies: spiral, galaxies: kinematics and dynamics, methods: numerical

1 INTRODUCTION

One of the most critical discoveries in recent years is the apparent co-evolution of central supermassive black holes (SMBHs) and their host galaxy spheroids. This phenomenon, often represented in scaling relations such as $M - \sigma$, $M_{\text{BH}} - M_{\text{bulge}}$, or $M_{\text{BH}} - L_{\text{bulge}}$, has been observed to hold over several orders of magnitude of SMBH mass and a variety of galaxy properties (e.g. Magorrian et al. 1998; Ferrarese & Merritt 2000; Gebhardt et al. 2000; Tremaine et al. 2002; Marconi & Hunt 2003; Häring & Rix 2004; Gültekin et al. 2009; Graham et al. 2011; McConnell & Ma 2013). Further observational campaigns suggest that these relations may evolve with redshift (Peng et al. 2006; Treu et al. 2007; Woo et al. 2008; Decarli et al. 2010; Bennert et al. 2011), though others refute this claim (Lauer et al. 2007; Volonteri & Stark

2011; Schulze & Wisotzki 2014). The $M - \sigma$ relation is a key constraint on any theory of the interplay between SMBH growth and galaxy evolution (e.g. Loeb & Rasio 1994; Haehnelt & Kauffmann 2000; Granato et al. 2001; Menou et al. 2001; Di Matteo et al. 2005; Wyithe & Loeb 2005; Croton et al. 2006; Micic et al. 2007; Hopkins et al. 2008; Tanaka & Haiman 2009; Volonteri & Natarajan 2009; Micic et al. 2011; Bellovary et al. 2013; Kormendy & Ho 2013). This relation is so well-accepted that both theoretical and observational studies use the $M - \sigma$ fit to scale the SMBH mass within a galaxy when not directly observable (Croton et al. 2006; Somerville et al. 2008; Wild et al. 2010). To build a theory of SMBH assembly in the context of galaxy evolution, it is clear that we need both accurate measurements of SMBH mass and bulge velocity dispersion, and a deep understanding of the biases and limits of these measurements.

Much scrutiny has been given to the difficulty of measuring SMBH masses, and for good reason; accurate mass

* E-mail: jillian.bellovary@vanderbilt.edu

measurements are very difficult and require a large investment of observational resources and careful analysis. However, measuring the velocity dispersion, σ , of a galaxy spheroid is also non-trivial. The galaxy orientation is imprinted on any observational measurement of σ , and unless we understand how this effect biases σ , we are at the mercy of the structure and viewing angle of every galaxy we observe. Velocity dispersions are commonly measured spectroscopically via the widths of stellar absorption lines, but it is difficult to isolate the light from spheroid stars from those of the disk. Every measurement of σ of the spheroid, therefore, will be contaminated by the kinematics of other galaxy components.

One way to examine the effect of orientation on measurements of σ is through simulations. A simulated galaxy can be rotated and viewed at any orientation, and can be analyzed to determine the intrinsic galaxy properties with no observational biases. We employ a sample of disk-dominated galaxies and examine how the viewing angle affects the apparent central velocity dispersion. We choose disk galaxies because the effects of orientation will be the most severe, and we wish to investigate the repercussions for the low-mass end of the $M - \sigma$ relation, which exhibits relatively large scatter. The scatter has been postulated to be due to evolutionary effects, such as merger history and environment (Kormendy et al. 2011; Micic et al. 2011; Mathur et al. 2012), and is dependent on galaxy mass, morphology, and bulge/disk ratio, among other things. However, another possibility is that some (or all) of the scatter is actually caused by orientation effects (Gebhardt et al. 2000), which include line-of-sight contamination from disk and halo stars as well as non-symmetric bulge effects and bulge rotation. It is thus critical to quantify the effect of viewing angle when measuring σ ; our understanding of how SMBHs and galaxies grow depends on it.

In this paper, we examine five disk-dominated simulated galaxies with a range of masses and bulge sizes. These galaxies are selected from “zoomed-in” cosmological simulations and have realistic star formation histories, baryon and gas fractions, and bulge and disk scale lengths. In § 2 we describe these simulations in detail, along with our methodology for measuring σ . In Sections 3 and 4 we present our results and discuss the repercussions for the observed $M - \sigma$ relation, respectively. We summarise the work in § 5.

2 SIMULATIONS AND VELOCITY DISPERSION MEASUREMENTS

We use the N -Body Smoothed Particle Hydrodynamics code GASOLINE (Stadel 2001; Wadsley et al. 2004) to create “zoomed-in” cosmological simulations of disk galaxies with a range of masses. A cosmological context is critical for this study, since it is important that galaxy bulges build naturally without assumptions as to the kinematics of the bulge or disk stars. We select our galaxies from a uniform, dark matter only 50 comoving Mpc box, and resimulate them using the volume renormalization method of Katz & White (1993) to better resolve our regions of interest. In a box of this size, the fundamental mode is nonlinear; while this effect changes the number and structure of the most massive halos, it has negligible effect on the centres of Milky Way galaxies.

Our gas, dark, and star particle masses are $m_{gas} = 2.7 \times 10^4 M_\odot$, $m_{dark} = 1.3 \times 10^5 M_\odot$, and $m_{star} = 8.0 \times 10^3 M_\odot$, respectively, and the force resolution is 174 pc. The initial conditions were generated with a WMAP 3 cosmology (Spergel 2007) and were run from $z = 150$ to $z = 0$. At $z = 9$, a uniform ionizing UV background appears, following the model of Haardt & Madau (2001). We identify individual galaxies using the tool AHF (Knollmann & Knebe 2009; Gill et al. 2004), which finds spherical overdensities with respect to the critical density. Changing the cosmology and reionization technique may affect the total luminosity function and formation time of low-mass halos, but has little effect on the spheroid velocity dispersion or bulge-to-disk ratios of our selected galaxies.

Gas cooling occurs via metal lines (described in Shen et al. 2010) and H_2 (Christensen et al. 2012). This low-temperature cooling, in combination with H_2 self-shielding and the dust shielding of HI and H_2 , allows gas to reach the high densities ($\rho \sim 100 \text{ amu cm}^{-3}$) and low temperatures ($\lesssim 1000\text{K}$) needed to appropriately model star formation in cosmological simulations (Governato et al. 2012). Star formation is dependent on the H_2 fraction (which itself depends on metallicity and the self-shielding ability of the gas). Star particles are born with a Kroupa IMF (Kroupa 2001), which dictates the occurrence of supernovae. Each supernova deposits 10^{51} erg of energy into the ISM within a blast radius described by McKee & Ostriker (1977). The gas particles within the blast radius have their cooling ability quenched until such time as the blastwave equations allow. This process mimics a supernova remnant through the snowplow phase and is described in detail in Stinson et al. (2006). We anticipate minimal effect of the choice of IMF or supernova feedback prescription on the structure and kinematics of the bulge in these galaxies. We do not include supermassive black hole physics in these simulations; we discuss the repercussions in Section 5. In short, while activity from supermassive black holes is expected to modify the central regions of galaxies, such phenomena are more pronounced among galaxies more massive than L_* (Fanidakis et al. 2013), and we do not expect a significant effect here.

From each simulation we use the primary galaxy at redshift $z = 0$, whose properties are detailed in Table 1. Our sample spans a range of $3 - 9 \times 10^{11} M_\odot$ in total mass and each galaxy has a prominent bulge and disk (see Figure 1 for examples). We focus on disk galaxies because elliptical galaxies will have less variation in their velocity dispersion measurements due to orientation effects, and we are specifically interested in the low mass end of the $M - \sigma$ relation. All of the systems we study are relaxed at $z = 0$ (for an interesting analysis of measuring σ in merging galaxies see Stickley & Canalizo (2013)). The five simulated galaxies for which we measure bulge velocity dispersion have made previous appearances in the literature in Zolotov et al. (2012); Loebman et al. (2012); Christensen et al. (2012); Munshi et al. (2013); Christensen et al. (2014). GASOLINE has proven to simulate galaxies with realistic baryon fractions and stellar masses for their halo mass (Munshi et al. 2013), bulge and disk properties (Brooks et al. 2011; Christensen et al. 2012, 2014), satellite distributions (Zolotov et al. 2012; Brooks & Zolotov 2014), and which follow the observed Kennicutt-Schmidt relation (Christensen et al. 2012). One

Table 1. Simulation Properties

Run	N within $R_{vir}(x10^6)$	M_{vir} ($10^{11}M_{\odot}$)	M_{star} ($10^{10}M_{\odot}$)	R_{vir} (kpc)	R_{eff} (kpc)
(1)	(2)	(3)	(4)	(5)	(6)
h239	17.2	9.13	4.50	250	2.16
h258	15.3	7.74	4.46	237	2.01
h277	13.9	6.79	4.24	227	2.41
h285	16.6	8.82	4.56	248	4.00
h603	21.8	3.43	0.78	181	3.77

Column 1: Simulation name. Column 2: Number of particles

within R_{vir} . Column 3: Total mass within R_{vir} . Column 4: Stellar mass within R_{vir} . Column 5: The virial radius R_{vir} .

Column 6: R_{eff} in the V band measured for a face-on orientation.

of our simulations, h603, was previously shown by (Christensen et al. 2014) to lie along the bulge scaling relations, demonstrating that the bulge has the appropriate size and surface brightness with respect to its host galaxy. We are confident that our simulations realistically represent galaxy bulges and disks, and offer an excellent setting to explore orientation effects on bulge properties.

2.1 Theoretical Measurements of Kinematics and Shape

One clear advantage of our galaxy models is that we can kinematically select the bulge stars and measure their dispersion and ellipticities. We kinematically decompose each galaxy by first identifying the stellar disk. We orient the coordinate system so that the angular momentum axis points along the z -axis and calculate J_z , the angular momentum of each star in the $x-y$ plane. We compare J_z to J_{circ} , the angular momentum the star would have if it were on a circular orbit with the same energy. We designate disk stars as having $J_z/J_{circ} \geq 0.8$, and spheroid stars as having minimal rotation. Using the entire matter distribution (gas, stars, and dark matter), we calculate the total energy for each particle in order to differentiate halo stars from the bulge. Bulge stars have higher binding energy than halo stars, and are distinguished by being within the radius where the mass profile of the spheroid changes slope.

After kinematically identifying the bulge, we centre it in position and velocity and determine the half-mass radius. The stars within this radius are those for which we measure σ_{tot} ; however, we exclude stars with a radius of 0.3 kpc (see Section 2.2 and Figure 2). We calculate velocity in the x , y , and z directions for each star particle. Summing the variance of these quantities gives us the square of the “true” velocity dispersion, σ_{tot} , measured directly from the simulation. We expect the three-dimensional dispersion to be a factor of $\sqrt{3}$ smaller than a one-dimensional line-of-sight value for an isotropic spheroid, and so we list the quantities σ_{tot} and $\sigma_{tot}/\sqrt{3}$ in Table 2. We also measure the intrinsic shape by calculating the moment of inertia tensor at the half mass radius. Our bulges are extremely realistic, and are consistent with the measurements made by Christensen et al. (2014) which show that the bulges obey the observed scaling relations relating surface brightness, magnitude, and size.

Table 2. Comparison of Theoretical and Observed Measurements

Run	Theoretical σ_{tot}	Theoretical σ_{los}	Median σ_{los}	Median σ_{los} (no rotation)	Shape (b/a)
(1)	(2)	(3)	(4)	(5)	(6)
h239	191.7	110.7	145.9	118.0	0.95
h258	193.8	111.9	165.5	115.3	0.60
h277	190.5	110.0	153.8	108.0	0.85
h285	217.2	125.4	135.5	133.1	0.88
h603	91.6	52.9	64.4	52.4	0.97

Column 1: Simulation. Column 2: Theoretical velocity

dispersion σ_{tot} in km s^{-1} . Column 3: $\sigma_{tot}/\sqrt{3}$ in km s^{-1} .

Column 4: Median σ_{los} in km s^{-1} as calculated by Equation 1.

Column 5: Median σ_{los} in km s^{-1} as calculated by Equation 2.

Column 6: Intrinsic shape.

2.2 Synthetic Observations of Kinematics and Shape

We have developed a process which closely mimics the observational method for determining σ_{los} from long-slit spectroscopy. To capture the effect of orientation on the line-of-sight σ_{los} measurement, we centre each galaxy in position and velocity space, and then rotate the galaxy along a series of angles, mimicking various lines of sight. We define two angles, θ and ϕ , which are measured in the polar and azimuthal directions, and rotate the galaxy in increments of 11.25 degrees in θ and ϕ to obtain a total of 512 different lines of sight.

For each orientation, we estimate the surface brightness by treating each star particle as a stellar population with a Kroupa IMF. Using the Starburst99 population synthesis code (Leitherer et al. 1999), we input the age and metallicity of each particle and receive magnitudes in several optical bands. We do not include dust obscuration, but we expect that neglecting dust will have minimal effect (see Section 5 for more discussion). By converting the V band magnitudes to luminosities, we sum over all the stars to obtain the surface brightness. We then fit a series of concentric ellipses to the surface brightness and measure the effective radius, R_{eff} , as described in Binney & Merrifield (1998) equation 4.18. We measure our bulge quantities using all of the stars in the galaxy which fall along the two-dimensional projection within an ellipse with semi-major axis R_{eff} . We present the R_{eff} for a face-on orientation for each galaxy in Column 6 of Table 1.

For each rotation, we then align a slit along the major axis of the rotated bulge. The slit has a width of 50 pc, which corresponds to $1''$ at 10 Mpc, though varying this width has negligible effect on our results. We divide the slit into 50 bins and measure the mean radial velocity (v_{los}) and the dispersion (σ) for each. Our results are also insensitive to the number of bins, as long as this number is greater than ~ 5 .

We then integrate along the slit, from $-R_{eff}$ to R_{eff} , using two methods. Historically, studies have combined the velocity standard deviation σ with the line of sight velocity v_{los} in accordance with the virial theorem, e.g. as in Gültekin et al. (2009):

$$\sigma_{los}^2 = \frac{\int (\sigma(r)^2 + v_{los}(r)^2) I(r) dr}{\int I(r) dr}, \quad (1)$$

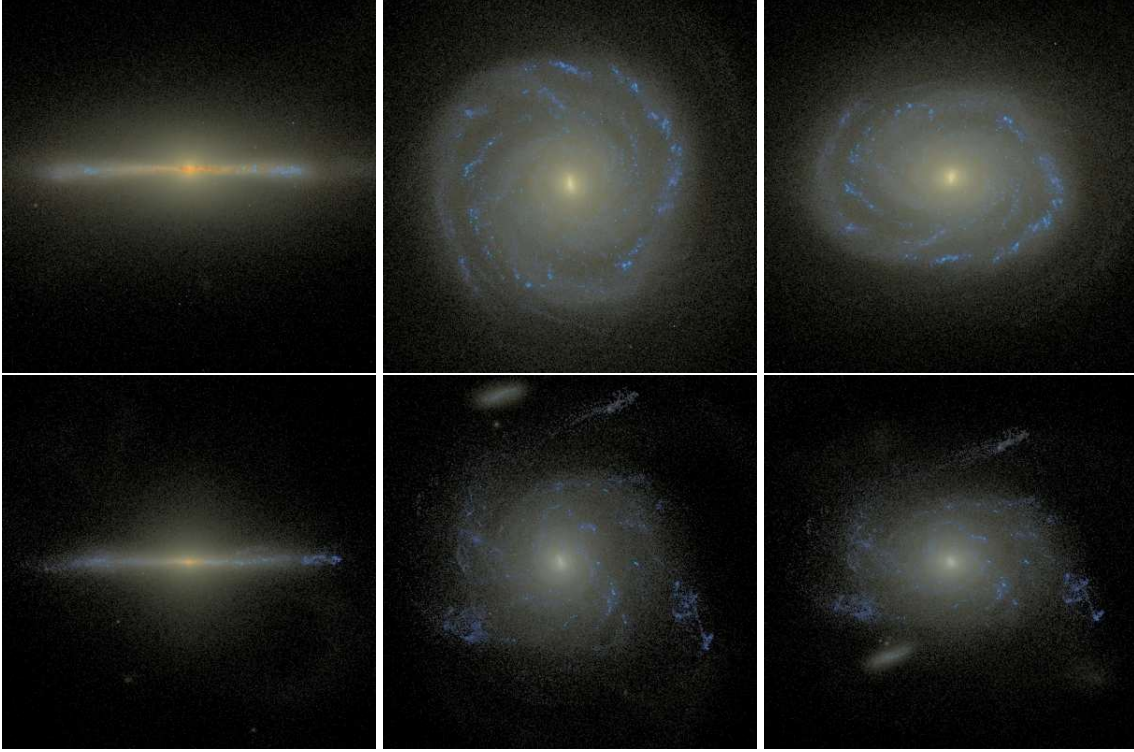


Figure 1. *Top row, Left:* Edge-on SDSS *gri* image of Milky Way-like galaxy *h258*, created with Sunrise (Jonsson 2006). *Centre:* Face-on image. *Right:* Image of galaxy inclined at 45 degrees. *Bottom row:* The same for less-massive galaxy *h603*. The size of each image is 40 kpc across.

where $I(r)$ is the surface brightness. However, a recent study by Woo et al. (2013) suggests that for systems with substantial rotation (such as the disk galaxies we focus on here), the contribution of v_{los} inflates the overall velocity dispersion. In an attempt to mitigate this bias, the authors instead suggest using the more basic equation:

$$\sigma_{\text{los}} = \frac{\int \sigma(r) I(r) dr}{\int I(r) dr} \quad (2)$$

for systems with a rotational component (see also Kang et al. 2013). It is not clear, however, that ignoring the rotational or anisotropic component of a virialized bulge would be appropriate to track a theoretical link between the SMBH mass and the kinematics of the bulge. For this reason, in this work we primarily focus on the first method, but discuss how using Equation 2 affects our results. In Figure 2 we present our slit measurements of σ_{los} (as calculated in Equation 1) and v_{los} for every galaxy orientation (grey lines) for the simulation *h258*. We show the median and standard deviation with red and blue curves, respectively. While these profiles are qualitatively similar to those presented in observational papers, the central region of the velocity dispersion profile is not well-represented due to the resolution limitations of our simulations. We bracket the region with the central dip (which is about $\sim 15\%$ of R_{eff}) with red dashed lines in Figure 2. This distance from peak to peak corresponds to a radius of ~ 1.8 softening lengths (or 0.3 kpc). According to Figure 2, the stars in this region are not reliable for kinematic study; we exclude this area from both our theoretical and synthetic observation velocity dispersion measurements. We have tested our method by excluding ranges of 1, 2, and

3 times the softening, and find that 1.8 is an appropriate factor to maximize meaningful information while excluding that which is unreliable. See §5 for a discussion of resolution concerns.

We note that the bulges identified by our kinematic decomposition and synthetic observations are not identical; each process selects the bulge component based on different criteria. At the moment it is not clear whether either method is “correct” for measuring fundamental scaling relations such as $M - \sigma$. We assert that observations of σ_{los} may have a large scatter due to galaxy orientation, and that simulations can help us explain the source of this scatter, in part by determining the σ from the kinematically-selected bulge.

3 RESULTS

The distribution of σ_{los} measurements (using Equation 1) as a function of orientation of each galaxy is shown in Figure 3. The red vertical lines are the medians of each distribution, and the blue hatched regions are the highest and lowest 10% values. The theoretically calculated line-of-sight velocity dispersion is denoted by the vertical green dashed line for each case. The distribution is non-Gaussian for every galaxy, and is skewed toward high σ_{los} . The fact that the distribution is not Gaussian is disturbing; the effects of inclination cause the *apparent* velocity dispersion to vary by several tens of km s^{-1} , with a strong bias toward larger values. The spread of values is around 0.3 dex, consistent with what is observed in $M - \sigma$ scatter (Gültekin et al. 2009). Thus, these variations

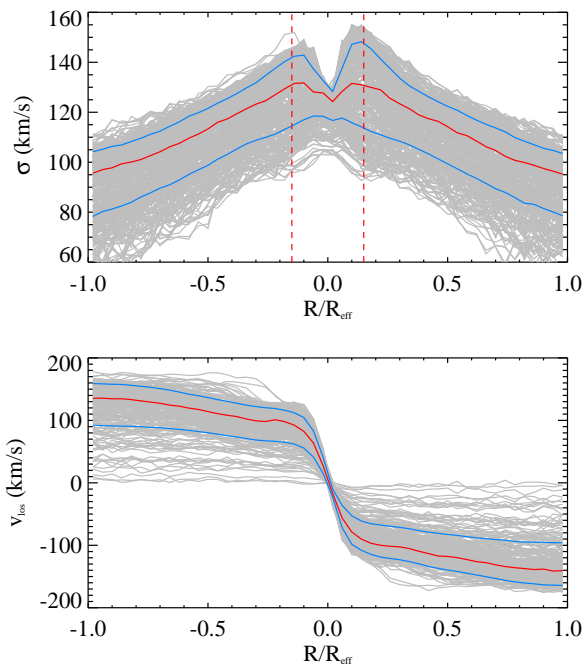


Figure 2. Profiles of σ_{los} (top) and v_{los} (bottom) from our simulated slit measurements for galaxy *h258*. Grey lines represent measurements for the full range of orientations, red lines are the medians, and blue lines are the mean $\pm 68\%$. The vertical dashed lines in the top panel represent regions where resolution effects prevent an accurate measurement of σ , so we neglect that region of the slit.

may be a principal source of scatter in the low-mass end of the observed $M - \sigma$ relation. The scatter is larger than the stated observational measurement errors, hinting that the wide spread in the low-mass end of the $M - \sigma$ relation may be caused by evolutionary effects, or by an underestimate of the measurement errors, or both (Harris et al. 2014). *We recommend that measurement errors for velocity dispersions of bulges in disk galaxies should never be estimated at less than 20 km s^{-1} , simply due to orientation.*

The use of Equation 2, with the rotational velocity component removed, has a marked difference for galaxies with a noticeable rotational component. In Table 2 we list the median values of σ_{los} for both observational methods, and in Figure 4, we show the distribution of σ_{los} calculated with both methods for two examples. The distribution without rotation (blue line) is shifted to lower values for galaxy *h277* (left panel), indicating that the inclusion of rotational velocities contributes substantially to σ_{los} . The distribution is also far narrower, suggesting that the additional rotational motions substantially broaden the range of possible observed values. On the other hand, galaxy *h285* (right panel) does not have substantial rotation in its central region, so the distributions are indistinguishable. Of our five galaxies, only *h285* lacks significant rotation in the central component; the other four all show a decrease of up to 25% in their median σ_{los} values when Equation 2 is used. Overall, the method of Equation 2 is successful at isolating purely dispersion-dominated motions, while Equation 1 represents the contribution of the full kinematic system. In terms of the $M - \sigma$ relation, it remains to be seen which equation is a better

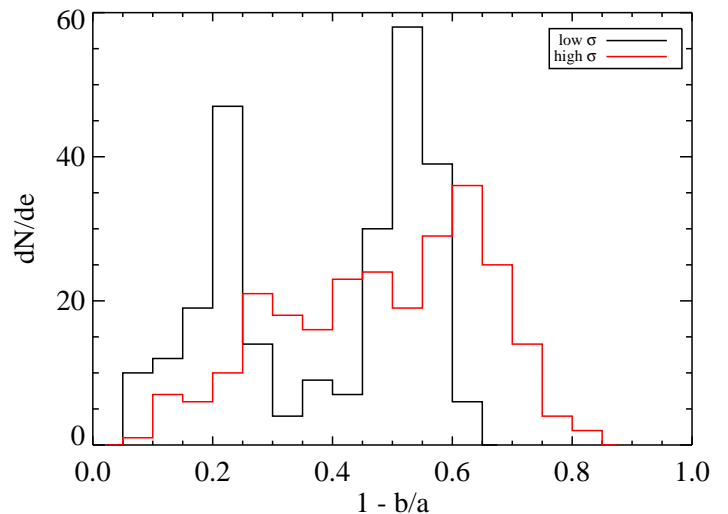


Figure 5. Distribution of ellipticities for the combined galaxy sample. The black histogram is for the 10% lowest values of each galaxies' σ_{los} distribution, and the red line is for the 10% highest. Face-on galaxies have characteristically lower values of σ_{los} , while for edge-on galaxies σ_{los} is higher.

metric to decipher how SMBHs and their host bulges are interrelated (see Woo et al. (2013) for more details).

In Table 2 we compare the theoretical velocity dispersions, σ_{tot} and $\sigma_{\text{tot}}/\sqrt{3}$, to those measured by synthetic observations. Comparing the median observed velocities for both methods (with and without rotation) to the theoretical value, we see that the simulation value is larger than the “observed” value, which is in turn larger than the observed value neglecting rotation. Our estimates of $\sigma_{\text{tot}}/\sqrt{3}$ fall within the extreme low end of most of the line-of-sight measurements. While this result could be because the bulges are not perfectly spherical or isotropic, the major factor is very likely a large population of non-bulge stars contaminating the line of sight for the synthetic observations. Since it is impossible to isolate the bulge light from a two-dimensional photometric projection, this contamination factor will always be present.

The observed measurement of σ_{los} with no rotation is characteristically lower (by $\sim 20\%$) than the traditional method, which is due to lack of inclusion of stars with rotational components to their motion. The bulges of late-type galaxies have non-negligible rotation, with the exception of *h285*; in this case the line-of-sight methods match each other. Notably, the measurement without rotation is very close to the one-dimensional theoretical measurement. Since both methods purposely exclude rotational motions, it is reasonable that they should roughly agree. Using Equations 1 and 2 together give us an idea of how rotation- vs dispersion-dominated a spheroid is; further studies with such considerations may give us more clues on how SMBHs grow and evolve with respect to the evolution of their hosts.

Because observations quantify galaxy inclination as a single measurement based on galaxy shape, rather than specific (and arbitrary) angles θ and ϕ , we report ellipticity (defined as $1 - b/a$, where a and b are the projected axis ratios) as a proxy for galaxy orientation. We measure the axis ratio b/a at the distance where the semi-major axis a of our surface brightness ellipse fits equals R_{eff} . In Figure

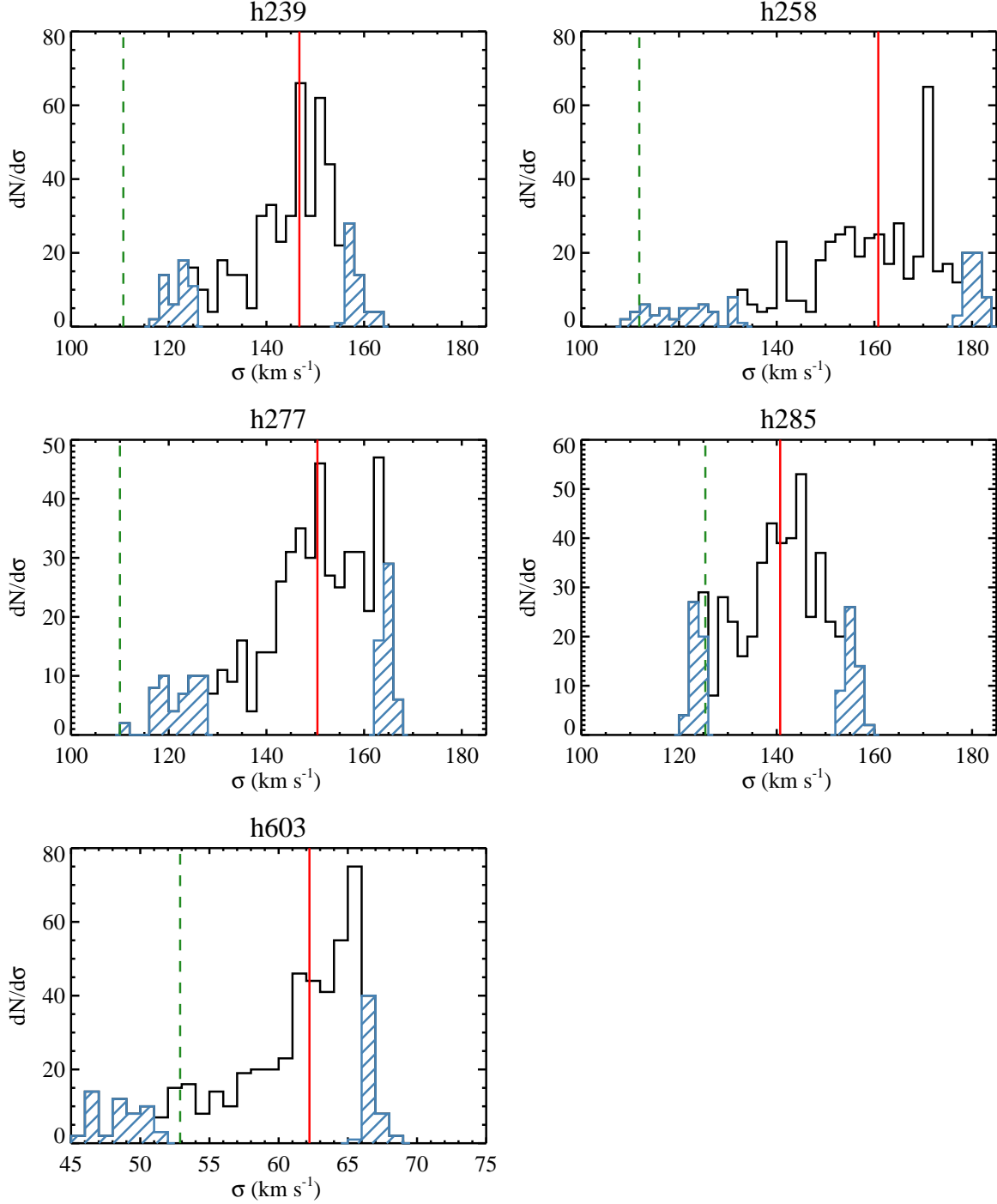


Figure 3. Distribution of measurements of σ_{los} for every line of sight for all five galaxies. The blue hatched regions are the lower and upper 10% of the distributions, and the red vertical line is the median of each distribution. The vertical green dashed line is the value of $\sigma_{\text{tot}}/\sqrt{3}$ derived directly from the simulations (see §2.1).

5, we show the distribution of ellipticities for the combined galaxy sample, for only the 10% highest (red histogram) and lowest (black histogram) values of each galaxy’s σ_{los} . The highest values of σ_{los} are seen at all orientations, with perhaps a slight bias toward more edge-on inclinations. The lowest values, on the other hand, have a bimodal distribution divided between face-on orientations and those which are more moderately inclined. The effect of lower dispersions

for face-on galaxies and higher for edge-on ones may be partially explained by the fact that when looking through a highly inclined galaxy, one is peering through a large quantity of disk stars in addition to those of the bulge. This geometrical argument has also been made by Brown et al. (2013), who studied the velocity structure of collisionless simulations of disk galaxies using an integral field method. Contamination by line-of-sight disk stars has been quanti-

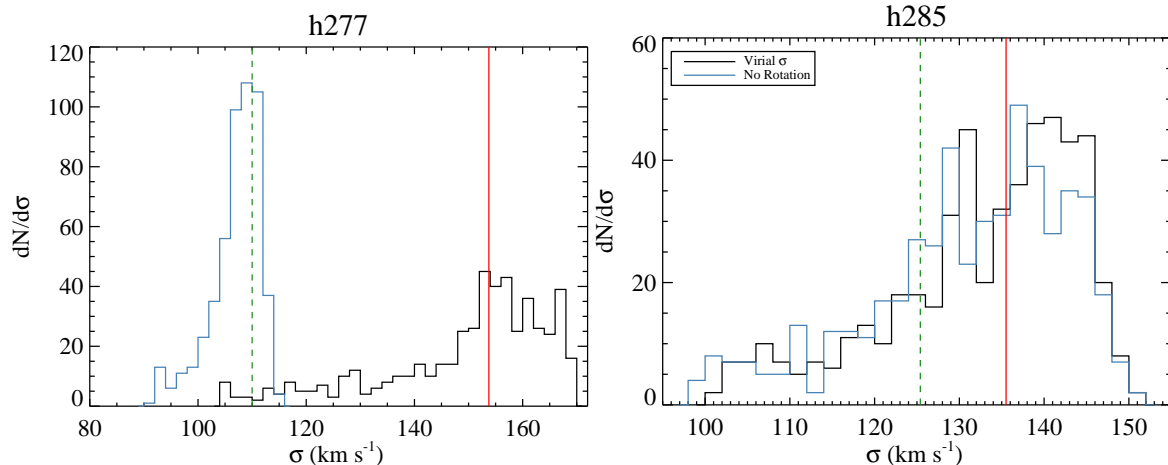


Figure 4. *Left:* Distribution of σ_{los} calculated using Equation 1 (black) and Equation 2 (blue) for simulation *h277*. The solid red line indicates the median of the measured distribution, while the dashed green line is the theoretically measured line of sight value (see Section 2.1). *Right:* The same for simulation *h285*. The median for *h277* is shifted to lower values when the rotational component is removed. However, *h285* has no rotational component in the central region, so its σ_{los} profile is unchanged.

fied by Hartmann et al. (2013), who suggest that a highly-inclined system artificially boosts σ_{los} values by 25%; our results agree with this assessment. Including these extraneous rotational velocities may artificially inflate the observed dispersion, and currently there is no method to isolate and subtract the contaminants from the dispersion-dominated population. However, the situation is more complicated than this simple argument states, since there is also a population of low dispersion measurements at higher ellipticities. These measurements may stem from non-axisymmetric bulge shapes, which may dominate the ellipticity measurement even in a face-on system. Using a larger radius to measure ellipticity, to encompass more of the disk, we obtain similar results.

The relationship between velocity dispersion and orientation is not straightforward – in Figure 6, we plot ellipticity vs velocity dispersion for all 512 lines of sight for each galaxy (black points). While the points fall within a general envelope, there is no overall trend between σ_{los} and ellipticity. The red line shows the mean σ_{los} for ellipticity bins of 0.1, and the vertical error bars denote one standard deviation from the mean. Even the shapes of these curves are not consistent from galaxy to galaxy. At moderate inclinations ($0.2 < e < 0.6$), measurements of σ_{los} can differ by several tens of km s^{-1} for a given ellipticity. We highlight this fact in the lower right panel, which shows the dispersion in σ_{los} vs ellipticity for each of the five galaxies. Each galaxy displays a large spread in σ_{los} at moderate inclinations, but the peaks vary from $0.2 < e < 0.6$. The only regime where σ_{los} is relatively constant is in the highly inclined case. In addition, we plot the intrinsic shape with the theoretically calculated $\sigma_{\text{tot}}/\sqrt{3}$ as a coloured asterisk in Figure 6 for each galaxy. In four out of five cases, the point representing the theoretical measurement falls outside of the locus of observational data. The combination of projection effects and line of sight contamination from other galaxy components renders observationally determining intrinsic galaxy properties extremely difficult.

Despite these efforts, each galaxy has unique trends and there seems to be no simple way to estimate a correction

for a measured σ_{los} of a galaxy given its inclination. We do caution observers to take care when estimating σ_{los} for moderately inclined disk galaxies (which is unfortunately the majority). The range of measurements varies by several tens of km s^{-1} at these orientations, and thus σ_{los} and any subsequent estimated quantity must have correspondingly large uncertainties.

4 REPERCUSSIONS FOR THE $M - \sigma$ RELATION

Thus far we have demonstrated that observational measurements of σ_{los} may not be as reliable as previously thought. This revelation has many repercussions regarding galaxy dynamics and evolution. In this section we focus on the effects on the observed $M - \sigma$ relation.

The low-mass end of the observed $M - \sigma$ relation has larger scatter than the higher-mass end (Hu 2008; Gültekin et al. 2009; Gadotti & Kauffmann 2009; Greene et al. 2010). A common explanation for the scatter is simply hierarchical evolution; as galaxies and black holes grow over time, they increase in mass together and more tightly adhere to their scaling relations (Peng 2007; Jahnke & Macciò 2011). Lower-mass galaxies in particular have likely undergone fewer major mergers, and the above argument may not even apply (Kormendy et al. 2011). SMBH fueling in isolated disk galaxies is likely triggered by secular, stochastic processes such as disk or bar instabilities (Cisternas 2011; Kocevski 2012; Simmons et al. 2013; Athanassoula 2013), which may not result in measurable trends between SMBHs and galaxy spheroids. Evolutionarily speaking, the larger scatter for both σ and black hole mass for late-type galaxies is expected.

However, the orientation effects presented in this paper may be able to account for almost the entirety of the scatter alone. The distributions of σ_{los} have a width of several tens of km/s , and correspond to about 0.3 dex, which is approximately the amount of scatter seen in the low-mass $M - \sigma$ relation. We show how this scatter translates to a scatter

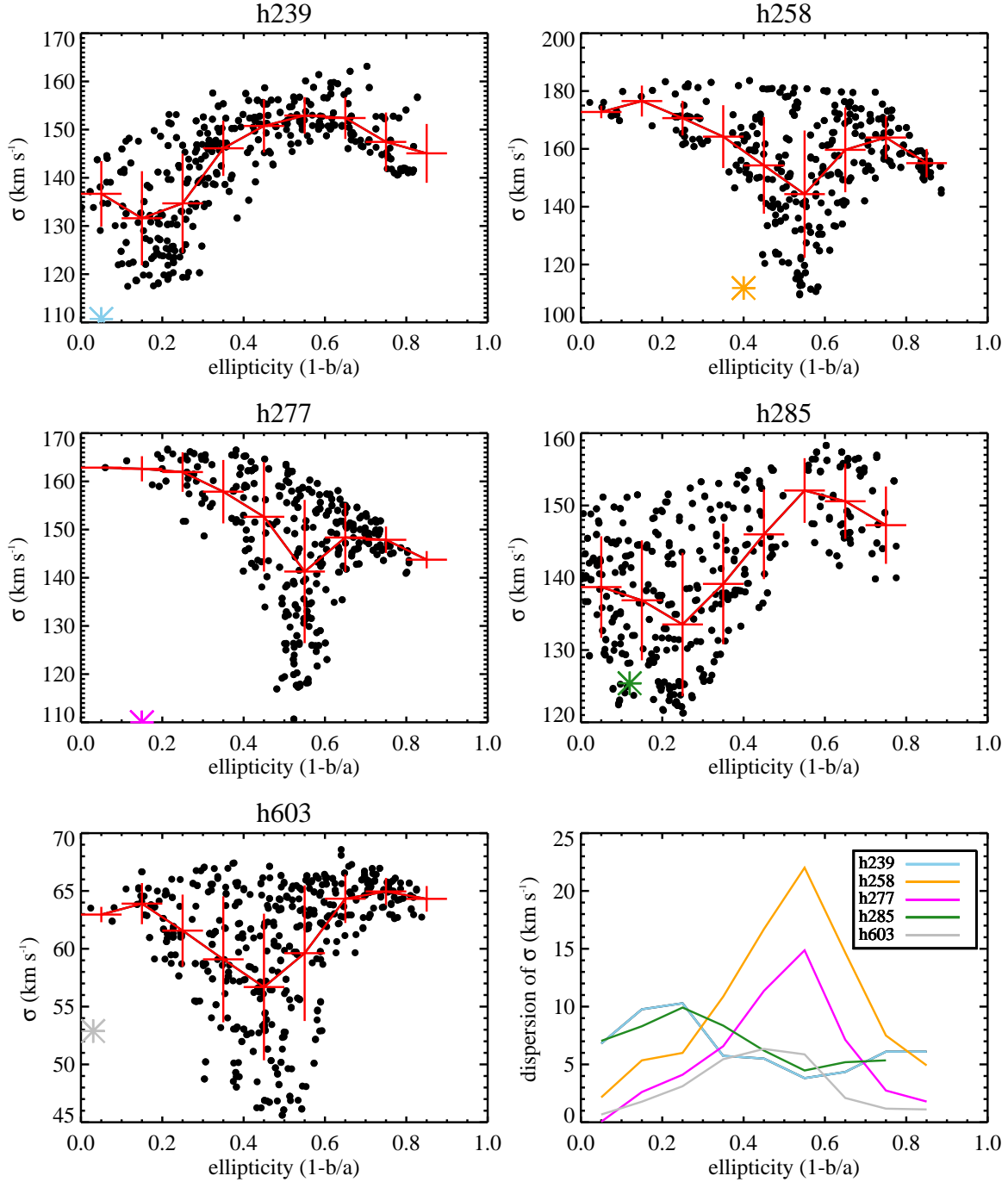


Figure 6. Ellipticity vs σ_{los} for every line of sight in each of the five galaxies. The red line passes through the mean value of σ_{los} for bins of 0.1 in ellipticity, and the errors represent one standard deviation. Coloured asterisks are the theoretically calculated values of e and σ_{los} (see Section 2.1). In the lower right panel, we plot the dispersion of σ_{los} vs ellipticity for each galaxy. Moderate inclinations exhibit the most variation in measuring σ_{los} .

in estimated black hole mass in Figure 7; using the relation from McConnell & Ma (2013), we input the values of σ_{los} for each line of sight to obtain M_{BH} . The values of M_{BH} span about an order of magnitude. This wide scatter serves as a warning that estimates of black hole masses from σ_{los} measurements may have much larger errors than previously assumed (e.g. 0.33 dex in Shankar et al. (2004)) for late-type galaxies. Conversely, theoretical studies wishing to compare

to the observed $M - \sigma$ relation must take care to measure σ_{los} in a way that is consistent with observational methods.

In Figure 8, we depict the expected scatter in the context of the $M - \sigma$ relation. We randomly draw 10^6 values of σ_{los} for each galaxy from the measured distributions, and assign a black hole mass based on the late-type relation from McConnell & Ma (2013). We include the intrinsic scatter in black hole mass as well as the uncertainty in their fit to create the distribution represented by the coloured con-

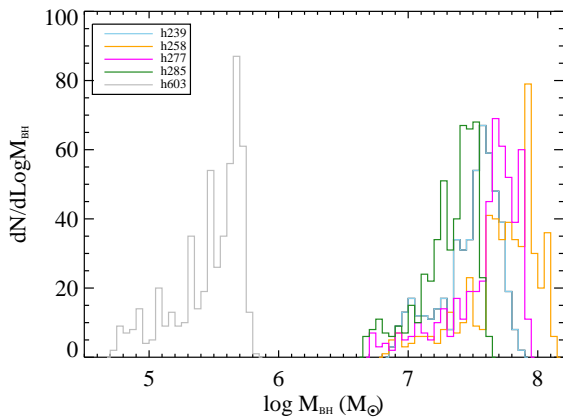


Figure 7. Distribution of black hole masses for each measurement of σ_{los} , using the relation from McConnell & Ma (2013) to convert from σ_{los} to M_{BH} . There is about an order of magnitude in the spread of the estimated masses.

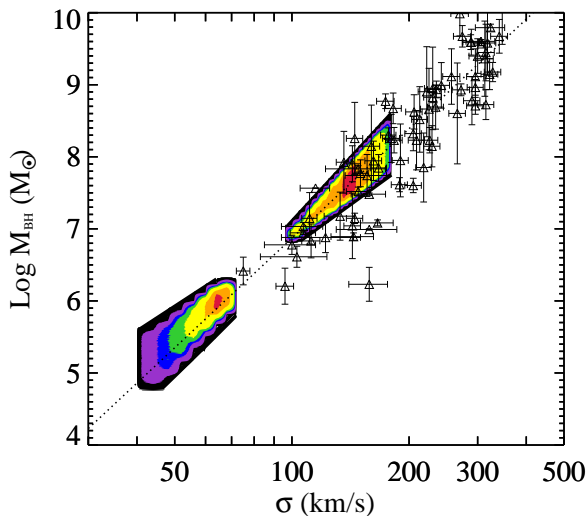


Figure 8. Predicted scatter in the $M - \sigma$ relation based on the possible range of measured velocity dispersions. We randomly draw 10^6 values of σ_{los} for each galaxy, and assign a black hole mass based on the late-type relation from McConnell & Ma (2013). We include the intrinsic scatter in black hole mass as well as the uncertainty in their fit to create the distribution represented by the coloured contours (coloured by point density). The black points and black dotted line represent the data and late-type fit to the data from McConnell & Ma (2013).

tours (coloured by point density). Overplotted on the figure are data points from McConnell & Ma (2013). The scatter of the observational data is comparable to, but somewhat larger than, the spread of the simulations, indicating that evolutionary effects may have a role to play as well, and that the scatter may not be due solely to orientation effects. Still, orientation may play a substantial role in the scatter of the low-mass end of the $M - \sigma$ relation.

5 DISCUSSION AND CONCLUSIONS

While this work has focused on repercussions for the $M - \sigma$ relation, our simulations do not include black hole physics

such as accretion and feedback. We do not expect this exclusion to have a significant effect; our galaxy sample is at a low enough mass that black hole feedback effects do not dominate over other processes. SMBH feedback does affect star formation in the bulge region, and it is possible that our velocity dispersion measurements are characteristically large due to neglecting SMBH feedback quenching. In fact, the bulge/disk ratios in these simulated galaxies may already be larger than expected compared to observations (Christensen et al. 2014); if SMBH feedback reduces the size of the bulge relative to the disk, our results concerning contamination from disk stars are likely strengthened. Regardless, we do not expect our result of asymmetric σ_{los} distributions due to orientation to be changed in any way, since the asymmetry is primarily caused by contamination from disk stars and not by intrinsic bulge properties.

We also do not include the effects of internal dust extinction and reddening when calculating surface brightness. Stickley & Canalizo (2012) employ a simple model for dust extinction and find that significant dust presence can lead to a modest decrease ($\sim 13\%$) in the measured value of σ_{los} . Since dust preferentially affects edge-on orientations, it is possible that for these lines of sight the observed σ_{los} would be lower. We do not expect any of our galaxies to be heavily obscured, however, and so our results will not be affected strongly.

In §2 we discuss eliminating the central region of each simulated galaxy from our analysis for resolution reasons. That this step is necessary is unfortunate, because in observations the highest signal-to-noise region is the centre. The centre dominates observational measurements and there is no way to compensate for its loss in a simulation with finite resolution. However, the main points of our results are not affected by this issue. We treat the theoretical measurements and synthetic observations in the same manner, excluding the region from both, which assures we are making valid comparisons. In addition, the behaviour of σ_{los} out to R_{eff} is well-behaved outside of the excluded region (Figure 2), suggesting that the majority of the data is of high quality. We have also verified that increasing the slit width (by up to a factor of 10) and adjusting the length of the slit (by factors of a few in either direction) bring no quantitative changes to our findings. While the magnitude of our σ_{los} measurements may be slightly underestimated because we are missing the very peak of the central distribution, the rest of our results are still solid.

We caution the use of measurements of σ_{los} in late-type galaxies to derive bulk galaxy properties. In fact, any global correlation that relies on σ , such as the Fundamental Plane, will be biased. The variation due to orientation alone is $\sim 20 \text{ km s}^{-1}$, and the inability to eliminate disk stars from an observational measurement introduces a contamination which artificially increases σ_{los} . The method of Woo et al. (2013) may mitigate this effect somewhat; however, if a bulge has a rotational component, the full kinematics will not be properly accounted for. Since the relationship between orientation and σ_{los} is not straightforward, there is no simple way to correct for this effect. Ellipticities of $0.2 < e < 0.6$ are the most strongly affected by large σ_{los} variations; unfortunately, a large fraction of late-type galaxies fall into this category.

In summary, using state-of-the-art high resolution cos-

mological simulations of disk galaxies, we quantify the effect of galaxy orientation on the measurement of bulge velocity dispersion. We carefully designed our measurements to closely mimic observational methods, and found that the value of σ_{los} is highly dependent on viewing angle. The distribution of σ_{los} is asymmetric and skewed toward higher values, which correspond to more inclined orientations. The scatter in σ_{los} of ~ 0.3 dex is approximately equal to that of the low-mass end of the $M - \sigma$ relation, suggesting that orientation may substantially contribute to the scatter. Estimates of black hole masses using scaling relations such as $M - \sigma$ must be taken with extreme caution in this range, as the spread in σ_{los} corresponds to a 1.0 dex variation in black hole mass.

ACKNOWLEDGMENTS

Simulations were run using computer resources and technical support from NAS. JMB and KHB acknowledge support from NSF CAREER award AST-0847696. FG acknowledges support from HST GO-1125 and NSF AST-0908499. SL acknowledges the Michigan Society of Fellows for financial support. CRC acknowledges support from NSF grants AST-0908499 and AST-1009452. We are grateful to Jon Bird and Rololfo Montez for helpful discussions.

REFERENCES

- Athanassoula E., 2013, Bars and secular evolution in disk galaxies: Theoretical input. p. 305
- Bellovary J., Brooks A., Volonteri M., Governato F., Quinn T., Wadsley J., 2013, *ApJ*, 779, 136
- Bennert V. N., Auger M. W., Treu T., Woo J.-H., Malkan M. A., 2011, *ApJ*, 742, 107
- Binney J., Merrifield M., 1998, *Galactic Astronomy*
- Brooks A. M., Solomon A. R., Governato F., McCleary J., MacArthur L. A., Brook C. B. A., Jonsson P., Quinn T. R., Wadsley J., 2011, *ApJ*, 728, 51
- Brooks A. M., Zolotov A., 2014, *ApJ*, 786
- Brown J. S., Valluri M., Shen J., Debattista V. P., 2013, *ApJ*, 778, 151
- Christensen C., Governato F., Quinn T., Brooks A. M., Fisher D. B., Shen S., McCleary J., Wadsley J., 2012, *ArXiv e-prints*
- Christensen C., Quinn T., Governato F., Stilp A., Shen S., Wadsley J., 2012, *MNRAS*, 425, 3058
- Christensen C. R., Brooks A. M., Fisher D. B., Governato F., McCleary J., Quinn T. R., Shen S., Wadsley J., 2014, *MNRAS*, 440, L51
- Cisternas M. e. a., 2011, *ApJ*, 726, 57
- Croton D. J., Springel V., White S. D. M., De Lucia G., Frenk C. S., Gao L., Jenkins A., Kauffmann G., Navarro J. F., Yoshida N., 2006, *MNRAS*, 365, 11
- Decarli R., Falomo R., Treves A., Labita M., Kotilainen J. K., Scarpa R., 2010, *MNRAS*, 402, 2453
- Di Matteo T., Springel V., Hernquist L., 2005, *Nature*, 433, 604
- Fanidakis N., Georgakakis A., Mountrichas G., Krumpe M., Baugh C. M., Lacey C. G., Frenk C. S., Miyaji T., Benson A. J., 2013, *MNRAS*, 435, 679
- Ferrarese L., Merritt D., 2000, *ApJL*, 539, L9
- Gadotti D. A., Kauffmann G., 2009, *MNRAS*, 399, 621
- Gebhardt K., Bender R., Bower G., Dressler A., Faber S. M., Filippenko A. V., Green R., Grillmair C., Ho L. C., Kormendy J., Lauer T. R., Magorrian J., Pinkney J., Richstone D., Tremaine S., 2000, *ApJL*, 539, L13
- Gill S. P. D., Knebe A., Gibson B. K., 2004, *MNRAS*, 351, 399
- Governato F., Zolotov A., Pontzen A., Christensen C., Oh S. H., Brooks A. M., Quinn T., Shen S., Wadsley J., 2012, *MNRAS*, 422, 1231
- Graham A. W., Onken C. A., Athanassoula E., Combes F., 2011, *MNRAS*, 412, 2211
- Granato G. L., Silva L., Monaco P., Panuzzo P., Salucci P., De Zotti G., Danese L., 2001, *MNRAS*, 324, 757
- Greene J. E., Peng C. Y., Kim M., Kuo C.-Y., Braatz J. A., Impellizzeri C. M. V., Condon J. J., Lo K. Y., Henkel C., Reid M. J., 2010, *ApJ*, 721, 26
- Gültekin K., Richstone D. O., Gebhardt K., Lauer T. R., Tremaine S., Aller M. C., Bender R., Dressler A., Faber S. M., Filippenko A. V., Green R., Ho L. C., Kormendy J., Magorrian J., Pinkney J., Siopis C., 2009, *ApJ*, 698, 198
- Haardt F., Madau P., 2001, in Neumann D. M., Tran J. T. V., eds, *Clusters of Galaxies and the High Redshift Universe Observed in X-rays Modelling the UV/X-ray cosmic background with CUBA*
- Haehnelt M. G., Kauffmann G., 2000, *MNRAS*, 318, L35
- Häring N., Rix H., 2004, *ApJL*, 604, L89
- Harris G. L. H., Poole G. B., Harris W. E., 2014, *MNRAS*
- Hartmann M., Debattista V. P., Cole D. R., Valluri M., Widrow L. M., Shen J., 2013, *ArXiv e-prints*
- Hopkins P. F., Hernquist L., Cox T. J., Kereš D., 2008, *ApJS*, 175, 356
- Hu J., 2008, *MNRAS*, 386, 2242
- Jahnke K., Macciò A. V., 2011, *ApJ*, 734, 92
- Jonsson P., 2006, *MNRAS*, 372, 2
- Kang W.-R., Woo J.-H., Schulze A., Riechers D. A., Kim S. C., Park D., Smolcic V., 2013, *ApJ*, 767, 26
- Katz N., White S. D. M., 1993, *ApJ*, 412, 455
- Knollmann S. R., Knebe A., 2009, *ApJS*, 182, 608
- Kocevski D. D. e. a., 2012, *ApJ*, 744, 148
- Kormendy J., Bender R., Cornell M. E., 2011, *Nature*, 469, 374
- Kormendy J., Ho L. C., 2013, *ARAA*, 51, 511
- Kroupa P., 2001, *MNRAS*, 322, 231
- Lauer T. R., Tremaine S., Richstone D., Faber S. M., 2007, *ApJ*, 670, 249
- Leitherer C., Schaerer D., Goldader J. D., González Delgado R. M., Robert C., Kune D. F., de Mello D. F., Devost D., Heckman T. M., 1999, *ApJS*, 123, 3
- Loeb A., Rasio F. A., 1994, *ApJ*, 432, 52
- Loebman S. R., Ivezić Ž., Quinn T. R., Governato F., Brooks A. M., Christensen C. R., Jurić M., 2012, *ApJL*, 758, L23
- Magorrian J., Tremaine S., Richstone D., Bender R., Bower G., Dressler A., Faber S. M., Gebhardt K., Green R., Grillmair C., Kormendy J., Lauer T., 1998, *AJ*, 115, 2285
- Marconi A., Hunt L. K., 2003, *ApJL*, 589, L21
- Mathur S., Fields D., Peterson B. M., Grupe D., 2012, *ApJ*, 754, 146
- McConnell N. J., Ma C.-P., 2013, *ApJ*, 764, 184

- McKee C. F., Ostriker J. P., 1977, *ApJ*, 218, 148
- Menou K., Haiman Z., Narayanan V. K., 2001, *ApJ*, 558, 535
- Micic M., Holley-Bockelmann K., Sigurdsson S., 2011, *MNRAS*, 414, 1127
- Micic M., Holley-Bockelmann K., Sigurdsson S., Abel T., 2007, *MNRAS*, 380, 1533
- Munshi F., Governato F., Brooks A. M., Christensen C., Shen S., Loebman S., Moster B., Quinn T., Wadsley J., 2013, *ApJ*, 766, 56
- Peng C. Y., 2007, *ApJ*, 671, 1098
- Peng C. Y., Impey C. D., Rix H.-W., Kochanek C. S., Keeton C. R., Falco E. E., Lehár J., McLeod B. A., 2006, *ApJ*, 649, 616
- Schulze A., Wisotzki L., 2014, *MNRAS*, 438, 3422
- Shankar F., Salucci P., Granato G. L., De Zotti G., Danese L., 2004, *MNRAS*, 354, 1020
- Shen S., Wadsley J., Stinson G., 2010, *MNRAS*, 407, 1581
- Simmons B. D., Lintott C., Schawinski K., Moran E. C., Han A., Kaviraj S., Masters K. L., Urry C. M., Willett K. W., Bamford S. P., Nichol R. C., 2013, *MNRAS*, 429, 2199
- Somerville R. S., Hopkins P. F., Cox T. J., Robertson B. E., Hernquist L., 2008, *MNRAS*, 391, 481
- Spergel D. N. e. a., 2007, *ApJS*, 170, 377
- Stadel J. G., 2001, PhD thesis, AA(UNIVERSITY OF WASHINGTON)
- Stickley N. R., Canalizo G., 2012, *ApJ*, 747, 33
- Stickley N. R., Canalizo G., 2013, *ArXiv e-prints*
- Stinson G., Seth A., Katz N., Wadsley J., Governato F., Quinn T., 2006, *MNRAS*, 373, 1074
- Tanaka T., Haiman Z., 2009, *ApJ*, 696, 1798
- Tremaine S., Gebhardt K., Bender R., Bower G., Dressler A., Faber S. M., Filippenko A. V., Green R., Grillmair C., Ho L. C., Kormendy J., Lauer T. R., Magorrian J., Pinkney J., Richstone D., 2002, *ApJ*, 574, 740
- Treu T., Woo J., Malkan M. A., Blandford R. D., 2007, *ApJ*, 667, 117
- Volonteri M., Natarajan P., 2009, *MNRAS*, 400, 1911
- Volonteri M., Stark D. P., 2011, *MNRAS*, 417, 2085
- Wadsley J. W., Stadel J., Quinn T., 2004, *New Astronomy*, 9, 137
- Wild V., Heckman T., Charlot S., 2010, *MNRAS*, 405, 933
- Woo J.-H., Schulze A., Park D., Kang W.-R., Kim S. C., Riechers D. A., 2013, *ApJ*, 772, 49
- Woo J.-H., Treu T., Malkan M. A., Blandford R. D., 2008, *ApJ*, 681, 925
- Wyithe J. S. B., Loeb A., 2005, *ApJ*, 634, 910
- Zolotov A., Brooks A. M., Willman B., Governato F., Pontzen A., Christensen C., Dekel A., Quinn T., Shen S., Wadsley J., 2012, *ApJ*, 761, 71

This paper has been typeset from a \LaTeX file prepared by the author.